Charge trapping effects in CCDs for GAIA astrometry

L. Lindegren (21 Sept 1998)

1 Introduction

GAIA aims at an astrometric accuracy of about 10 μas at 15th magnitude. At the level of individual CCD read-outs, the corresponding image centroiding accuracy is about 200 μas, or 0.05 μm for a focal length of 50 m. It is hoped that the 'accuracy floor' for bright stars is a few times better than this, or say 0.01 μm for the individual centroiding. This means that the residual systematic errors, after very careful and extensive geometric and photometric calibration of all parts of the instrument, should be less than about 10^{-3} of a pixel.

It is known that the photon flux and the density of stars on the sky are in principle more than sufficient to calibrate the geometry of the CCDs to such an accuracy, even considering that each pixel column must be separately calibrated. However, this assumes that there is a stable geometrical quantity (the mean centroid shift) that can be calibrated. To the extent that the mean centroid shift depends on several other factors, such as the current signal and background levels, time, or even the past history of illumination, the shift becomes in practice impossible to calibrate. It is to the level of such 'random' shifts that the millipixel requirement applies.

In this connection it should be recalled that the electronic image of a 15th magnitude star, when it reaches the serial register, typically contains $\sim 10^4$ electrons in the central pixel column. The faintest detected stars give mages of ~ 100 electrons, but then the accuracy requirements are also relaxed by a factor 10.

Charge transfer inefficiency (CTI) has been identified as a potentially serious problem for very precise image centroiding in GAIA. Normally CTI is thought of as a linear effect, i.e. a certain (fixed) fraction ϵ of the charges are left behind when the charge package has been moved by one pixel. ϵ is called the CTI and $1 - \epsilon$ the CTE (charge transfer efficiency). Typically $\epsilon \sim 10^{-6}$ to 10^{-5} for undamaged CCDs. (We will, for the time being, only consider the parallel charge transfer along a TDI column, since the GAIA measurements are most sensitive to centroid shifts in that direction.) The linear CTI is discussed in Section 2.

Potentially much more troublesome are the highly non-linear CTI effects that are caused by charge trapping. The silicon layer in which the charge packets are transported (the buried channel) contains localised points in which electrons may be captured and re-emitted at a later time. The deferred charge is noted as an increased CTI. Traps may be caused by chemical impurities or, more importantly for space applications, by displacements in the crystal lattice produced by the impacts of energetic particles, typically protons. Because of the limited number of traps encountered by the charge packets, the trapping is not proportional to the signal, but the effect is rather to reduce the signal by a certain amount, i.e. a kind of thresholding. The resulting effect on the signal packets depends also very much on the background level.

1

There is an extensive literature on radiation-induced CTI in buried-channel CCDs, covering both experimental results and theoretical modelling of the effect. References and additional background information are well summarised in a recent paper by Hardy et al. (1998). That paper also describes a simple physical model capable of reproducing quite well measured CTI values and their variations with radiation level, temperature and signal level. The model described in Section 3 is to a large extent based on that paper.

While the increased CTI is perhaps the most easily measured effect of the charge trapping, it is the corresponding centroid shift which is most relevant for astrometry and GAIA. This effect is (to my knowledge) hardly at all discussed in the literature. Very roughly one can perhaps assume that the centroid shift is proportional to the CTI, but a detailed investigation of the effect through adequate modelling is clearly motivated.

2   Linear CTI

In this section we consider briefly the centroid shift associated with a linear (proportional) CTI, i.e. where a fixed fraction ϵ of the charges are left behind in each pixel transfer. Let N be the number of pixels in the column and assume that the image illuminates exactly one pixel at a time with unit exposure during a TDI period. During the first TDI period, when the image is centred on the first pixel, the charge accumulated in the first pixel is therefore $f_{11} = 1$ (and zero everywhere else). After transfer by one pixel and light integration during the second TDI period, the expected contents of the first two pixels are:

$$f_{21} = \epsilon \,, \quad f_{22} = 1 + (1 - \epsilon) \,. \tag{1}$$

After the third TDI period, the expected pixel contents are:

$$f_{31} = \epsilon^2 \,, \quad f_{32} = [1 + 2(1 - \epsilon)]\epsilon \,, \quad f_{33} = 1 + (1 - \epsilon) + (1 - \epsilon)^2 \,. \tag{2}$$

Generally, after m TDI periods the content of the nth pixel is ($n \leq m$):

$$f_{mn} = \sum_{j=0}^{n-1} \binom{m+j}{m} \epsilon^m (1 - \epsilon)^j \,. \tag{3}$$

After N periods the leading charge packet is in the last row. The final transfer into the serial register gives the signal

$$S_0 = f_{NN}(1 - \epsilon) = (1 - \epsilon) + (1 - \epsilon)^2 + (1 - \epsilon)^3 + \cdots + (1 - \epsilon)^N \,. \tag{4}$$

The first trailing packet, after transfer to the serial register, contains the signal

$$S_1 = f_{N+1,N}(1 - \epsilon) = [(1 - \epsilon) + 2(1 - \epsilon)^2 + 3(1 - \epsilon)^3 + \cdots + N(1 - \epsilon)^N]\epsilon \,, \tag{5}$$

while the second and third trailing packets contain, respectively,

$$S_2 = f_{N+2,N}(1 - \epsilon) = [(1 - \epsilon) + 3(1 - \epsilon)^2 + 6(1 - \epsilon)^3 + \cdots + \frac{(N + 1)N}{1 \cdot 2}(1 - \epsilon)^N]\epsilon^2 \tag{6}$$

and

$$S_3 = f_{N+3,N}(1-\epsilon) = [(1-\epsilon)+4(1-\epsilon)^2+10(1-\epsilon)^3+\cdots+\frac{(N + 2)(N + 1)N}{1 \cdot 2 \cdot 3}(1-\epsilon)^N]\epsilon^3 \,, \tag{7}$$

and so on. Naturally all the charges are eventually transferred to the serial register, so $S_0 + S_1 + S_2 + \cdots = N$.

ϵ being a small quantity, we might neglect terms of order ϵ^2 and higher to obtain

$$S_0 \simeq N - \frac{(N+1)N}{1 \cdot 2}\epsilon\,, \quad S_1 \simeq \frac{(N+1)N}{1 \cdot 2}\epsilon\,, \quad S_k \simeq 0 \;\; (k > 1)\,. \tag{8}$$

If N is large we find that the fraction of deferred charges is approximately $N\epsilon/2$, and that (to first order in ϵ) they are all deferred to the first trailing pixel. To the lowest significant order in ϵ, the fraction of charges in the kth trailing pixel is $\simeq (N\epsilon)^k/(k+1)!$.

Since the process is assumed to be linear, the CTI effect on an arbitrary (electronic) PSF can be obtained through convolution with the kernel function S_k/N, $k = 0, 1, \ldots$. This will result in both a shift and a widening of the PSF. The shift of the centre of gravity of the PSF is simply obtained by calculating the centre of gravity of the kernel. To first order in ϵ, this shift is

$$\delta = \frac{N\epsilon}{2} \tag{9}$$

pixels. The RMS width of the PSF is increased quadratically by the RMS width of the kernel. Again to first order in ϵ, the RMS kernel width in pixels is

$$\sigma = \sqrt{\frac{N\epsilon}{2}}\,. \tag{10}$$

The CTI was here treated as a completely deterministic process. In reality the charge transport is stochastic and the number of deferred charges in each transfer should more properly be modelled as a binomial process. If the total number of charges is not very small, this can be approximated by a Poisson process. The number of charges calculated in the deterministic way is then simply the expected number of charges in the Poisson process. Since the photon detection is also a Poisson process, it follows that one can equivalently regard the linear CTI as a shift and widening of the *optical* PSF, before detection. The noise contribution from the stochastic nature of the CTI is therefore accounted for by the widening of the PSF by the kernel width, Eq. (10). This can be shown also by considering the RMS fluctuation of δ in Eq. (9) resulting from the Poisson noise of the deferred charges.

To summarise, the linear CTI produces a *constant* shift of the expected location of the image centroid, while the stochastic nature of the effect is equivalent to a *widening* of the PSF. For a constant CTI these effects are easily (and in fact automatically) calibrated in the data reductions. As long as the total effect is relatively small ($N\epsilon \ll 1$), the linear CTI will therefore not be a problem for GAIA.

3 Charge trapping: A Monte Carlo model

Models of the CTI degradation such as the one described by Hardy et al. (1998) allow to calculate the expected number of charges trapped and deferred, the fraction of filled traps as function of position in the substrate, and similar mean quantities. Such models could also be adapted to calculate the mean electronic PSF resulting in TDI mode, and hence

Figure 1: Schematic representation of the charge transfer across three successive pixels, and the capture/emission of charges by traps (shown as small circles). A four-phase CCD ($M = 4$) is assumed, i.e. with four gates (electrodes) per pixel. The horizontal layers represent a section of the buried channel at successive time steps. The figure illustrates several features of the adopted model: the fixed number and location of traps within the substrate; the gaussian-ellipsoidal charge density distribution of the packets (at low charge densities); the instantaneous transfer of packets from one step to the next (τ_1 to τ_2, etc); the capture of a single charge at a trap with a probability proportional to the local charge density; the spontaneous emission of the charge from a filled trap, independent of the charge density; and the diffusion of emitted charges to the nearest packet. Simultaneously with all this, new charges are added to the packets according to a Poisson process governed by the local detection rate (stellar PSF plus background).

the expected shift as function of trap density, background and signal levels. However, it is not obvious that such a treatment is sufficient for the present problem. With reasonable trap densities, the expected number of traps in the active part of a single TDI column will be rather small and may be constant over a considerable time, perhaps sufficient for empirical calibration of the shifts. Thus, while the model could predict the mean shift, i.e. the average over many different trap configurations, this is not necessarily representative for the shifts produced by a given, more or less fixed configuration of traps.

An obvious way to study the effects of charge trapping is by means of detailed numerical simulation. If this is done at the level of the capture and emission of individual charges by the individual traps, it is easy to consider for instance the stochastic trapping effects in a fixed configuration. This is the principle adopted for the present study.

Briefly, the simulations follow the build-up and transport of charges along the buried channel of a single TDI column (Figure 1). Traps are placed randomly throughout the volume at a given density. Each trap has two possible states: empty or filled (by one

electron). For each step of the charge transfer, the three-dimensional charge distribution is calculated and hence, for each trap, the probability that its state will be changed during the step. If the state is changed, through the capture or emission of an electron, the size of the charge packet is modified accordingly. At the end of the column, the resulting charge packets are recorded and the location of the star image is determined by means of a cross-correlation algorithm.

3.1 Notations, coordinates and units

SI units are used consistently. The geometry of the buried channel is described in rectangular coordinates with $x = 0$ at the beginning of the TDI column and increasing in the direction of charge transport. y is the coordinate along the pixel rows, with $y = 0$ at the centre of the considered column. z is the depth coordinate, again with z at the centre of the channel. For an M-phase CCD with N pixels along the column, there are MN gates equidistantly along x. Each gate defines an elementary rectangular volume $\Delta x \Delta y \Delta z$ of the buried channel. The charge transfer proceeds in discrete time steps, with $2M$ steps required for the transfer by one pixel (in one TDI period). At a given time step of the clock sequence, a charge packet will be constrained to $M - 2$ or $M - 1$ adjacent elementary volumes (cf. Figure 1). The charge density within the buried channel is generally written $n_e(t, x, y, z)$ [m^{-3}].

k	Boltzmann's constant, $k = 1.3807 \times 10^{-23}$ J K^{-1}
m_e	mass of electron, $m_e = 9.109 \times 10^{-31}$ kg
q	charge of electron, $q = 1.602 \times 10^{-19}$ A s
T	absolute temperature
A^*	effective Richardson constant, $A^* = 2.52 \times 10^6$ A m^{-2} K^{-2} for n-type $\langle 100 \rangle$ Si
σ_t	trapping cross section
E_t	trapping state energy level below the conduction band
n_0	doping concentration
n_e	local charge density at point (x, y, z) in the buried channel
N	number of pixels along the TDI column
M	number of phases in the charge transfer ($M = 3$ or 4 considered)
Δt	TDI period
τ	dwell time during a specific step of the charge transfer
p_c	probability of capture during the dwell time
p_e	probability of emission during the dwell time
S	size of the charge packet in electrons
$P(x)$	stellar point spread function (PSF), normalised such that $\sum_n P(x_n) = 1$, where x_n is the coordinate of the nth pixel
a	stellar signal size (number of electrons under the PSF)
b	background level (number of electrons per pixel)

3.2 Capture and emission probabilities

Let n_e be the charge density in the vicinity of a trap. If the trap is empty, the probability that it will capture an electron during the infinitesimal time interval dt is

$$dp = r_c dt \tag{11}$$

where

$$r_c = \sigma_t v_{th} n_e \tag{12}$$

is the capture rate. (In the literature, this is usually expressed in terms of the capture time constant $\tau_c = 1/r_c$.) Here σ_t is the trapping cross section and

$$v_{th} = \sqrt{\frac{3kT}{m_e}} \tag{13}$$

the mean thermal velocity of the electrons. If the trap is filled, the probability of emission is given by

$$dp = r_e dt \tag{14}$$

where

$$r_e = \frac{\sigma_t A^* T^2}{q} \exp(-E_t/kT) \tag{15}$$

is the emission rate. A^* is the effective Richardson constant and E_t the trapping state energy level. Considering both processes together, the probability that the trap is filled after time t is governed by the differential equation

$$\frac{dp}{dt} = r_c(1 - p) - r_e p \,. \tag{16}$$

The general solution, assuming that r_c and r_e are constants, is

$$p(t) = \frac{r_c}{r_c + r_e} + C \exp[-(r_c + r_e)t] \tag{17}$$

where C is a constant of integration.

The charge transfer is assumed to be such that the electron density distribution is constant during a certain time interval τ (the dwell time), before the charges are redistributed in the next step of the transfer. Let n_e be the charge density in the vicinity of a trap during the dwell time and consider how $p(t)$ changes during the dwell time, from $t = 0$ to τ.

If the trap is empty at the beginning of the dwell time, then $p(0) = 0$ and we find $C = -r_c/(c + r_e)$ in Eq. (17). At the end of the dwell time the probability that the trap is filled is

$$p(\tau) = \frac{r_c - r_c \exp[-(r_c + r_e)\tau]}{r_c + r_e} \equiv p_c \,, \tag{18}$$

which defines the effective probability of capture, p_c. Conversely, if the trap is filled at the beginning of the dwell time, then $p(0) = 1$ and $C = r_e/(c + r_e)$. At the end of the dwell time, the probability that the trap is filled becomes

$$p(\tau) = \frac{r_c + r_e \exp[-(r_c + r_e)\tau]}{r_c + r_e} \equiv 1 - p_e \,, \tag{19}$$

which defines the effective probability of emission, p_{e}. With $r_{\mathrm{tot}} = r_{\mathrm{c}} + r_{\mathrm{e}}$ these probabilities can also be written

$$p_{\mathrm{c}} = \frac{r_{\mathrm{c}}}{r_{\mathrm{tot}}} \left[1 - \exp(-r_{\mathrm{tot}}\tau) \right] , \tag{20}$$

$$p_{\mathrm{e}} = \frac{r_{\mathrm{e}}}{r_{\mathrm{tot}}} \left[1 - \exp(-r_{\mathrm{tot}}\tau) \right] . \tag{21}$$

3.3 Charge density model

The equilibrium charge density distribution in a given potential can be obtained by solving Poisson's equation. Since the potential is itself modified by the charges, both the potential and charge density must be solved simultaneously. Examples of such calculations are given in Hardy et al. (1998). The concentration profiles (Figure 6 in that paper) indicate that the distribution is approximately gaussian as long as the density is small. This corresponds to the (linear) density model

$$
\begin{aligned}
n_e(x,y,z) &= \frac{S}{(2\pi)^{3/2}\sigma_x\sigma_y\sigma_z} \exp\left[-\frac{1}{2}\left(\frac{x-x_0}{\sigma_x}\right)^2 - \frac{1}{2}\left(\frac{y}{\sigma_y}\right)^2 - \frac{1}{2}\left(\frac{z}{\sigma_z}\right)^2 \right] \\
&= S\,g(x,y,z)
\end{aligned}
\tag{22}
$$

where S is the total charge of the packet and g is the normalised gaussian density function. x_0 is the central coordinate of the packet along the TDI column (in the other coordinates the packet is centred on $y = z = 0$). The standard widths σ_x, σ_y and σ_z depend on the dimensions of the gate and the thickness of the buried channel and are assumed to be known.

The linear model (22) cannot be used when the charge density approaches the doping concentration, n_0, because of saturation effects which set in at that density. This can be seen clearly in Figure 6 of Hardy et al., where a doping density of $n_0 = 10^{22}$ m^{-3} was assumed in the centre of the buried channel. The total charge can however continue to grow by increasing the width of the density distribution in all three coordinates. A reasonable *ad hoc* model for the saturation process is

$$n_e(x,y,z) = \frac{n_0\,S'\,g(x,y,z)}{n_0 + S'g(x,y,z)} , \tag{23}$$

where the parameter S' must be adjusted to give the correct total charge S. Let us now consider how S' can be computed as function of S.

The total charge at which saturation sets in is determined by the number of donors in the ellipsoidal volume,

$$S_0 = (2\pi)^{3/2}\sigma_x\sigma_y\sigma_y n_0 . \tag{24}$$

Roughly speaking, the linear model (22) is valid if $S \ll S_0$, while $S \gg S_0$ gives a flattened (partially saturated) density function. In terms of the dimensionless quantity $u = S'/S_0$ the total charge is found to be

$$S = \iiint n_e(x,y,z)\,\mathrm{d}x\,\mathrm{d}y\,\mathrm{d}z = S_0 B(u) \tag{25}$$

where

$$B(u) = \sqrt{\frac{2}{\pi}} \int_0^\infty \frac{ur^2 \, \mathrm{d}r}{u + \exp(r^2/2)} \, . \tag{26}$$

We need the inverse of the function $B(u)$, i.e. $u(B)$. For given S we then have $S' = S_0 u(S/S_0)$, whereupon the charge density follows from Eq. (23).

It is possible to tabulate $B(u)$ once and for all by numerical integration of Eq. (26) and then obtain $u(B)$ by inverse interpolation. However, in the present simulations an approximate analytical method was used. It is easy to see that $u \ll 1$ (the linear case) gives $B(u) \simeq u$, while $u \gg 1$ (the saturated case) gives $B(u) \simeq (4/3\sqrt{\pi})(\ln u)^{3/2}$. One can then construct a formula which has the correct asymptotic form in these two cases, and provides a reasonable approximation in the transition region $u \sim 1$. The following formula was used:

$$u(B) \simeq B \cdot (1 + B^{0.8})^{-1.25} \cdot \exp\left[\left(\frac{3\sqrt{\pi}}{4} B\right)^{2/3}\right] \, . \tag{27}$$

3.4 Simulation process

In an M-phase CCD the transfer of the charge packets by one pixel requires $2M$ steps. In Figure 1 the duration (dwell time) of each step is denoted $\tau_1 \ldots \tau_8$. The sum of these equals the TDI period ($\Delta t = 0.31$ ms in the MMS design). It is assumed that the charge density function $n_e(x, y, z)$ remains constant during the dwell time and then changes instantaneously for the next step. This is reasonable because the time for the charge distribution to reach equilibrium is of the order of (pixel size)$/v_{\mathrm{th}}$, or nanoseconds, which is short compared with the dwell time. In the simulations the given TDI period can in principle be divided arbitrarily between the $2M$ dwell times.

Figure 2 is a block diagram of the simulation process. Together with Figure 1 this should be almost self-explanatory. Only a few additional remarks are given below.

The light detection is simulated by computing the expected number of detected photons during the TDI period,

$$\mathrm{E}(k) = [b + aP(x_n - \xi - vt)]/N \, , \tag{28}$$

where b is the background count rate (including dark current), a the intensity and ξ the location of the star image; $P(x)$ is the stellar point spread function, x_n the position of the pixel and v the scan rate. To each packet is then added a number of electrons, k, generated as a Poisson process with expectation $\mathrm{E}(k)$. To simplify the process, this is only done once per TDI step, rather than for the individual dwell periods. Since $P(x)$ includes the smearing due to the charge transfer over the TDI period, the end result will be very nearly the same. a and b are expressed in electrons per CCD crossing; hence the factor $1/N$ to give the expected counts per TDI period.

For a given column geometry (number of pixels, number of gates per pixel, pixel dimensions and channel depth) all charge packets are initially set to the given background level and they are localised under respective gates. Similarly, empty traps are placed randomly throughout the channel according to the given trap density. Separate initialisations of the random number generator are used for setting up the traps and for the subsequent
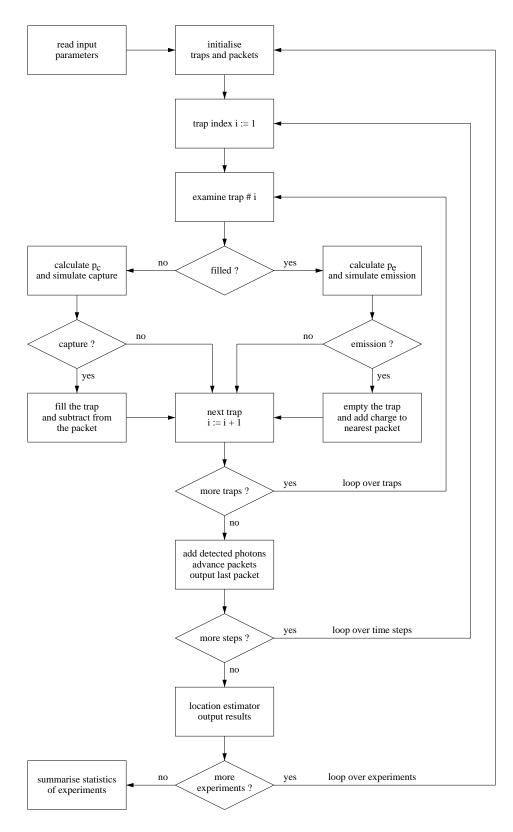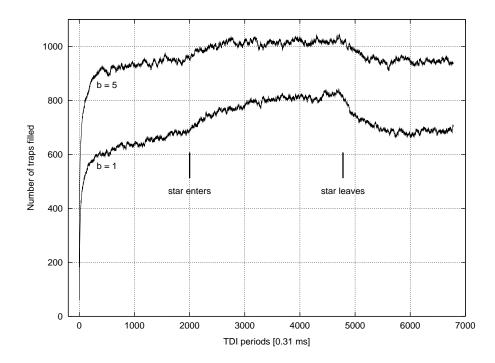
Figure 2: Block diagram of the simulation process.

Figure 3: Evolution of the total number of filled traps in the TDI column in two experiments with the same configuration of traps but different background levels, $b = 1$ and $b = 5$ counts per pixel. The image size is $a = 100000$ counts. Initially all traps are empty, but some are rapidly filled by the background count rate. As the star image enters the column, more traps are successively filled, presumably also those further from the centre of the channel. After the star image leaves, the number of filled traps returns to an equilibrium level. The time constant for this is about 0.1 s. Other parameters for the simulations are as in Table 1.

simulation of photon detection and charge trapping. In this way many different simulation experiments can be made for the same configuration of traps.

On output, the number of charges, S_j, in several successive packets around the expected centre of the image are recorded. The position ξ and size a of the stellar signal are estimated by a maximum cross-correlation method (the background b is assumed known). Only five successive pixel values S_j are used, centred on the highest value. Trigonometric interpolation of $P(x)$ is used to obtain the position at sub-pixel precision. The error in the location, $\xi_{est} - \xi_{true}$, and a_{est} are stored for subsequent statistical analysis.

Typically only the transit of a single star across the CCD is simulated. This requires a number of time steps (dwell periods) equal to $2MN$, where M is the number of phases and N the number of pixels. However, to correctly simulate the response to an isolated star requires that the traps have first reached an equilibrium state determined by the background rate b. Currently this is done by setting the star location ξ in (28) to such a large value that the simulation runs for a few thousand TDI periods with only the background, before the star image enters the CCD. The required time for equilibrium can be estimated by monitoring the total number of filled traps as a function of time (Figure 3 shows a few examples).

Table 1: Parameters used in the simulation experiments.

Description	Designation	Value
number of pixels	N	2780
number of phases	M	4
TDI period	Δt	0.31 ms
time steps during transfer	$\tau_1 = \tau_3 = \tau_5 = \tau_7$	77.5 μs
	$\tau_2 = \tau_4 = \tau_6 = \tau_8$	0
packet size parameters	σ_x	0.36 μm*
(* during odd time steps)	σ_y	2.00 μm
	σ_z	0.04 μm
doping concentration	n_0	10^{22} m^{-3}
temperature	T	200 K
cross section of trap	σ_t	6×10^{-19} m^2
energy level of trap	E_t	0.42 eV
density of traps	n_t	0, 10^{16} and 3×10^{16} m^{-3}

4 Simulation results

The numerical results presented below should be regarded as a first demonstration of the method, to be followed by more extensive experiments after reviewing and tuning the model and its parameters.

The assumed parameters are summarised in Table 1. The temperature, pixel size and number of pixels correspond to the current MMS design. The doping density and the packet size parameters σ_x, σ_y, σ_z were essentially estimated from Hardy et al. 1998, assuming that the packet size scales roughly with the dimensions of the gates. The trap characteristics (σ_t and E_t) were also taken from that paper, but they are similar to figures published elsewhere for the phosphorus vacancy complex.

The stellar point spread function $P(x)$ (at pixel resolution) was taken to be a very schematic (0.02, 0.04, 0.24, 0.40, 0.24, 0.04, 0.02), i.e. with 40 per cent of the energy falling in the central pixel, and so on. It should be noted that there is a roughly similar distribution of the energy in the perpendicular coordinates (i.e. into the adjacent columns), which needs to be considered for converting the signal sizes into stellar magnitude. For instance, a star of magnitude $G = 15$ produces a total of 29 400 electrons during a CCD crossing (0.86 s), half of which (or less, depending on the transverse smearing) may come from a single pixel column. Thus we can roughly take $a = 10^4$ to correspond to a 15th magnitude star. It is this a that is plotted on the horizontal scale in Figures 4 to 9. It should not be confused with the charge packet size, which of course increases during the integration, and reaches at most $0.40a$ at the end of the integration.

Figures 4 to 9 contain the main results of the simulations. For given trap density, a fixed (but initially random) configuration of traps was used, and batches of 10 simulations were made for each combination of signal size (a) and background level (b). The points in the

figures always represent the mean or standard deviation of the 10 individual simulations.

Figure 4 shows that a considerable systematic shift of the image occurs, especially for small signals (faint stars). As expected, the effect depends also on the background level and can be reduced by increasing the background. Figure 5 suggests that the shift is roughly proportional to the trap density. Assuming that the mean shift can be calibrated as function of a and b (and time), a more relevant quantity is the standard deviation of the shifts (Figure 6). This must be compared with the standard deviation obtained in the nominal case of no traps (Figure 7). The median ratio between the corresponding points in Figures 5 and 6 is 1.20 ± 0.07. Assuming that the added variance is proportional to the density of traps, we derive the following tentative formula for the increase in the astrometric standard error as function of trap density:

$$\frac{\sigma}{\sigma_0} = \sqrt{1 + \frac{n_t}{2 \times 10^{16} \ \mathrm{m}^{-3}}} \ . \tag{29}$$

Apart from the shift, the signal is also reduced by the trapped and deferred charges. This is shown in Figures 8 and 9, again for the standard trap density $n_t = 10^{16} \ \mathrm{m}^{-3}$. Clearly this will complicate the photometric calibration and introduce an additional error source in the photometry. The non-linearity of the charge deferral may also affect the capability to disentangle complex objects such as double stars.

5 Conclusion and future simulations

Tentatively, for the particular parameters assumed in the present simulations and without any special design features for reducing the effect, it appears that a maximum tolerable trap density is about $10^{16} \ \mathrm{m}^{-3}$. According to Hardy et al. (1998) such a trap density could be produced by a 3-MeV protons at a fluence of about 1.8×10^{13} protons m^{-2}. For 'standard' 10-MeV protons the same effect should be obtained by 5×10^{13} protons m^{-2} (using Fig. 1 in Dale et al. 1993).

As can be seen from the figures, the 10 simulations per parameter set is really an absolute minimum for getting any useful statistics at all. A major disadvantage of the present method is its computational slowness, and even the meager results shown here required several days of CPU time on a workstation. For future simulations several tricks could however be used to speed up the calculations, and we also consider the use of a much faster, multi-processor computer.

6 References

Dale C., Marshall P., Cummings B., Shamey L., Holland A. 1993, *Displacement Damage Effects in Mixed Particle Environments for Shielded Spacecraft CCDs*, IEEE Trans. Nuclear Sci. 40, 1628

Hardy T., Murowinski R., Deen M.J. 1998, *Charge Transfer Efficiency in Proton Damaged CCD's*, IEEE Trans. Nuclear Sci. 45, 154
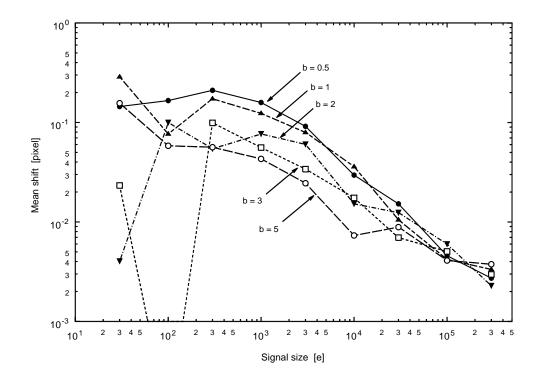
Figure 4: Mean shifts of the PSF profile due to charge trapping, as function of signal size a and background level b. Each point represents the average of 10 simulations with the same trap distribution. The shifts are expressed in pixels of 9 μm = 37 mas. The density of traps is $n_t = 1.0 \times 10^{16}$ m^{-3}.
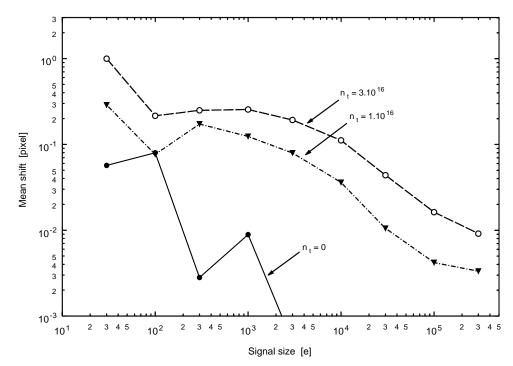

Figure 5: The mean shifts for $b = 2$ and three different trap densities: $n_t = 0$ (i.e. no traps: no shift is expected — the curve shows only the positive random fluctuations), $n_t = 10^{16}$ (as in Figure 4) and $n_t = 3 \times 10^{16}$ m^{-3}. The last two curves indicate that the shift is roughly proportional to the trap density.
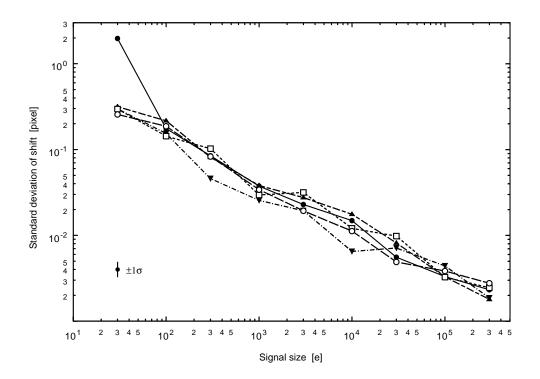
Figure 6: Standard deviations of the shifts in Figure 4, i.e. for trap density $n_t = 10^{16}$ m^{-3}. Each point is the sample standard deviation of 10 simulations and therefore has a relative uncertainty of $\pm 20^{-1/2}$ (shown by the error bars in the lower-left corner). The standard deviations are expressed in pixels of 9 μm $= 37$ mas. Symbols and line types have the same meaning as in Figure 4.
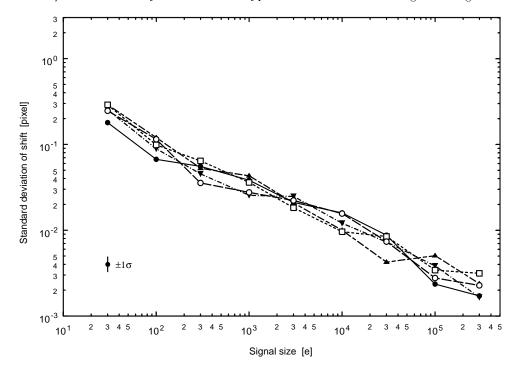

Figure 7: Standard deviations as in Figure 6, but without traps ($n_t = 0$). The mean shift of the curves between Figure 6 and this figure is about 20 per cent, which is the increase in the centroiding noise caused by the traps. This relative increase appears to be practically independent of signal size and background level.
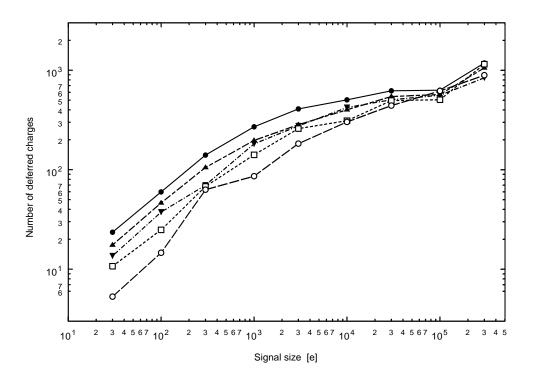
14

Figure 8: Number of deferred charges in the experiments of Figure 4 and 6. The number of deferred charges is defined as $a_{\mathrm{true}} - a_{\mathrm{est}}$, where a is the signal size in electrons.
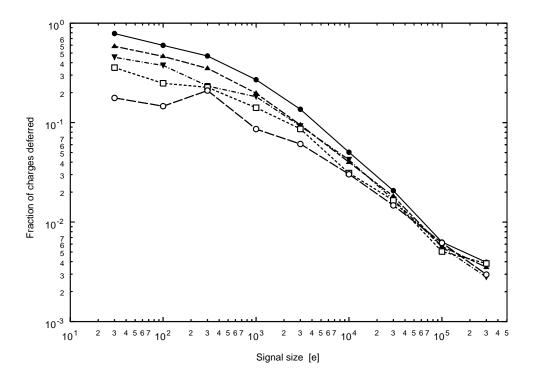

Figure 9: The same results as in Figure 8, but expressed as the fraction of deferred charges, $(a_{\mathrm{true}} - a_{\mathrm{est}})/a_{\mathrm{true}}$.